ISSN 1392–1207. MECHANIKA. 2020 Volume 26(1): 5–11

Numerical Investigation of AISI 4140 Powder High Relative Density Compaction in Terms of Compaction Velocity

Faruk GÜNER
Department of Mechanical Engineering, Giresun University, 28100, Giresun, Turkey, E-mail: faruk.guner@giresun.edu.tr

crossref http://dx.doi.org/10.5755/j01.mech.26.1.22862

1. Introduction

Machine and electronic parts manufactured by metal powder compaction have an increasing volume day by day. Especially, production of complex shaped and miniature parts by Powder Metallurgy (PM) are (known to be) more advantageous in terms of high production rates, cost-effectiveness, net shape qualities, (efficient use of materials), and easy operation opportunities [1]. Metal powder compaction parts are usually uniaxial MIM or PIM processed parts [2, 3].

AISI 4140 is a low alloy steel with high fatigue strength, toughness and impact resistance. With these features, it has been preferred in the production of complex and small shaped parts in areas such as automotive and defence industry. Bolts, belts, triggers, thumb pieces can be produced by MIM of AISI4140 [4,5]. In this study the problems encountered in the net shape production of these types of AISI 4140 metal powder parts were investigated numerically in terms of relative density and compaction velocity.

The cold compacted PM parts called "green body" may be sintered. Final relative density (RD) which is the ratio of particles to the total volume, including voids has an effect on the mechanical properties of compacted part [6]. MPFEM analysis in which cap material models utilized, showed that even if compaction process occurs in a wide range of mean stress, the elasticity of compacted products depends on density distribution, not the mean stress [7,8].

Compaction velocity, final density or contact interactions can be listed as the variables that can affect the mechanical properties [9]. Those variables which can be defined as academically uncertain, originate from the nature of pro-cess. For instance, compaction is assumed to be under a certain temperature. Besides, internal friction of moving particles generates heat that is very hard to investigate but it can be defined by kinetic equations. While the velocity of the particles changes the kinetic energy, it is important to determine different compaction velocities [4,10]. Researchers studied on high strain rate and high pressure loading of iron argued that the elastic-plastic transition may begin in low stress rates such as 100 MPa and, phase transition may occur in the moving surfaces [11]. Investigations over high velocity compaction showed that compaction velocity has a significant capacity to improve the mechanical properties of PM products. They also put forth that the micro cracking has an important role on yield stress [12]. The effects of high compaction velocity can be mathematically defined as differentiation of deformation mechanism in micro scale [13].

Both the RD and compaction velocity and the friction phenomenon are non-negligible issues on PM process. Since the friction phenomenon may differ in micro-size, it should have a response in the mechanical properties [14,15]. Some studies showed that particle-particle contacting coefficient of friction may be different from the particle-die contacting coefficient of friction [5,16].

Due to the fact that there were many parameters to be investigated, experimental studies were considered difficult and expensive. Numerical analyses were performed in order to provide preliminary information about experimental studies and industrial applications. Besides, numerical simulations offer scientific details about the processes that cannot be investigated easily by low cost.

There are various kinds of numerical analysis methods, i.e.; Finite Element Method (FEM), Discrete Element Method (DEM), Continuum Analysis, etc. FEM is a well-known method and Multi Particle Finite Element Method (MPFEM) is a special application of FEM to the particulate systems. All manufacturing process of PM such as loading, unloading or relief can be easily modelled in 2D or 3D by MPFEM [17]. DEM needs further developments in order to be utilized in complex engineering problems. Recent studies investigated the suitability of this method in analysing elastic behaviour or crack initiation and propagation of 3D heterogeneous continuous media. Besides it needs more accurate elastic coefficients comparing with FEM and fast Fourier based technique [18-20]. DEM is still being developed for simple non-spherical particle analyses [21-23]. In continuum analyses the part defined as a solid which have voids inside. Special material models have to be utilised and contact interactions were neglected [24-25].

In this study, the effects of compaction velocity and RD distribution on the AISI 4140 powder compaction pro-cess, suitable for complex shaped part production in defence industry, were investigated numerically using MPFEM. Analyses at different compaction velocities up to high RD values were investigated under certain conditions. The MPFEM model containing spherical particles in three different diameters were constructed in 2D. von Mises material model utilized to the analyses in this study. The MPFEM results were examined in stress distribution via high RD and compaction velocity.

2. The MPFEM model

2.1. Solid model

PM process analyses can be performed both 2D and 3D while it was possible to obtain sufficient engineering data from 2D analyses results [26].

The model should be treated carefully in order to simulate a realistic initial RD in 2D analyses. The use of particles with different diameters would be a suitable solution for capturing the required initial RD. It was impossible to achieve high RD (or volume ratios) without using particles of different diameters in industrial applications [27]. In

this context, a small control volume of rear sight base of a gun which was produced by powder compaction, modeled in 2D. Totally 123 particles, composed of 40 particles of 25 μm in radius, 44 particles of 35 μm in radius, 39 particles of 45 μm in radius, have been settled in die. The cross sectional area of the model was 0.715x0.905 mm. Fig. 1 shows the unmeshed 2D model accenting the three different diameter geometry and their random distribution. Random distribution was obtained by effecting gravity force to the particles in solid modelling computer aided design program.

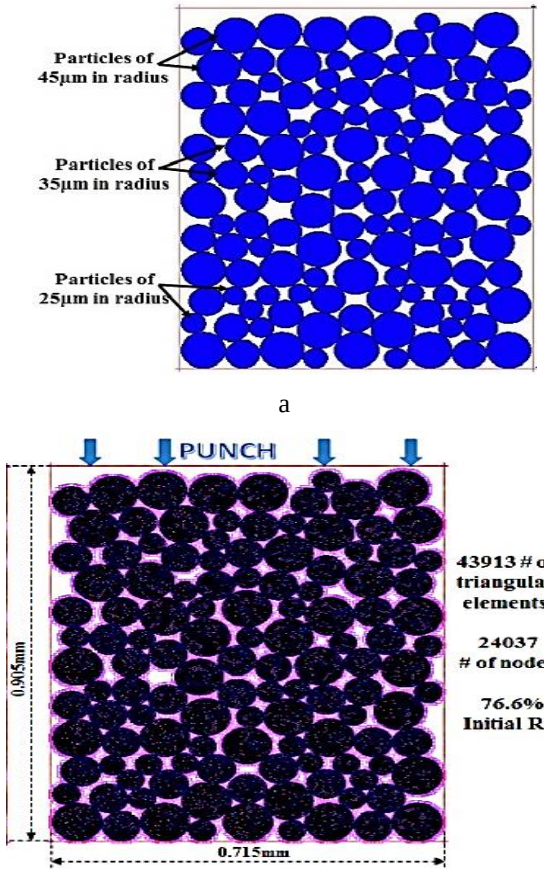

Fig. 1 2D model emphasizing particle distribution: a - unmeshed bodies of different diameters, b - meshed bodies of different diameters and initial conditions

The displacement or residual testing option was set in convergence testing in FEA. In the residual option, the software was testing whether the result of division of the largest residual force by the maximum reaction force was smaller than tolerance of 0.1. In the displacement option, the software was testing whether the actual displacement change of the increment was bigger or not comparing to the maximum displacement of the last iteration. If one of those options occurred, the convergence was satisfied. Full Newton-Raphson iterative procedure was performed in the implicit MPFEM analysis.

2.2. Material model

Although there were many forms of yield criteria available in literature, von Mises yield criterion was suitable for many problems due to the continuous nature of the function. von Mises yield criterion has a good agreement with deformation analysis of iron materials. This yield criterion indicates that if the equivalent stress was equal to the yield stress of uniaxial test, the material yields [28]. The stress can be expressed both in principal Cauchy stress or nonprincipal Cauchy stress that can be seen in Eqs. (1) and (2). In those equations σ is Equivalent von Mises stress, σ_1, σ_2, σ_3 are principal Cauchy stresses, σ_x, σ_y, σ_z, τ_{xy}, τ_{xz}, τ_{yz}, are nonprincipal Cauchy stresses, shear and normal stresses.

$$\sigma = \left[\left(\sigma_1 - \sigma_2\right)^2 + \left(\sigma_2 - \sigma_3\right)^2 + \left(\sigma_3 - \sigma_1\right)^2 \right]^{\frac{1}{2}/\sqrt{2}}, \quad (1)$$

$$\sigma = \left[\begin{array}{l} \left(\sigma_x - \sigma_y\right)^2 + \left(\sigma_x - \sigma_z\right)^2 + \left(\sigma_z - \sigma_y\right)^2 + \\ +6\left(\tau_{xy}^2 + \tau_{xz}^2 + \tau_{zy}^2\right) \end{array} \right]^{\frac{1}{2}/\sqrt{2}}. \quad (2)$$

In MPFEM, the equations have to be defined in matrix form to evaluate them in stiffness matrix. The matrix form of von Mises yield criterion was given in Eq. (3) where it was expressed in terms of deviatoric Cauchy stresses, σ_{ij}^d [28].

$$\sigma = \sqrt{\frac{3}{2}\sigma_{ij}^d \sigma_{ij}^d}, \quad (3)$$

$$\sigma_{ij}^d = \sigma_{ij} - \frac{1}{3}\sigma_{kk}\delta_{ij}. \quad (4)$$

In MPFEM analyses, the yield stress was calculated by the power function form of von Mises yield criterion which was given in Eq. (5) where A, B, m, n are material constants, σ_y, is the yield stress, ε, is the initial yield strain, $\bar{\varepsilon}$, is the equivalent strain, $\tilde{\varepsilon}$, is the equivalent strain rate [15].

$$\sigma_y = A\left(\varepsilon_0 + \bar{\varepsilon}\right)^m + B\tilde{\varepsilon}^n. \quad (5)$$

The power law form of von Mises yield criterion has been used in powder compaction analyses elsewhere in literature. Those samples were shown in Eqs. (6) and (7) [8]. The yield function used in MPFEM analyses of this study was given in Eq. (8). Elasticity modulus E, was 210 GPa, Poisson Ratio υ was 0.3 and other material constants of Eq. (8) were taken from literature [28].

$$\text{For steel, } \sigma_y = 640.9\left(\bar{\varepsilon}\right)^{0,38551} + 187, \quad (6)$$

$$\text{For iron powder, } \sigma_y = 508.8\left(\bar{\varepsilon}\right)^{0,39641} + 183, \quad (7)$$

$$\text{For 4140 powder, } \sigma_y = 650\left(\bar{\varepsilon}\right)^{0.0117} + 262\tilde{\varepsilon}^{0.15}. \quad (8)$$

2.3. Contact model

One of the main challenges of this study was the contact detection of 133 spherical particles touching each other and die. Node to segment contact type was utilized by FEA software package. In this type of contact, edges of other 2-D deformable bodies or segments from rigid bodies were accepted as segments and it was assumed that all of

these segments may come into contact with all nodes and other segments. The contact algorithms and further equations of FEA contact detection were detailed in Marc Mentat Volume A [27]. The contact detection algorithms were containing friction definition in which Amonton-Coulomb friction model with a constant coefficient of 0.05 was taken into account the MPFEM analyses.

3. Results and discussion

MPFEM analysis were performed via nine different compaction velocities in aim to investigate compaction velocity effect on high RD. The main examination was performed on Equivalent stress values and stress distribution via die height. The RD value reaches 95% at the end of the analysis by moving the punch 0.175 mm. Fig. 2 shows the RD change and particle distribution by the time increments. The particles were rearranged by the movement of the punch, therefore, obscure stresses were read in the first few increments. When the rearrangement of the particles were completed, sensible stress data obtained.

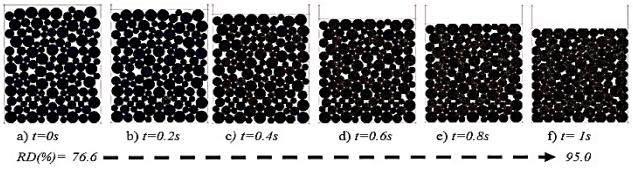

Fig. 2 RD change and particle distribution during MPFEM analysis

One of the main parameter examined in this study was the effect of compaction velocity. Different compaction velocities have been achieved by displacing the punch in same length and different duration. 0.00273, 0.0108, 0.0432, 0.175, 0.7, 2.8, 11.2, 44.8 and 179.2 mm/s compaction velocities were investigated via MPFEM analyses. Max. Eq. von Mises stresses of different punch velocities at the final increment were given in Fig. 3. Max. Eq. von Mises stress obtained for the lowest velocity was 925 MPa, while the highest compaction velocity stress value was 1180 MPa. Other values constitute almost a linear increasing trend. It can be seen in Fig. 3 that the Eq. von Mises stress has an increase of about 25% while compaction velocity has a much greater value of increase. It can be concluded that the mass production speed can cause unexpected stresses on compacting powders in industrial applications.

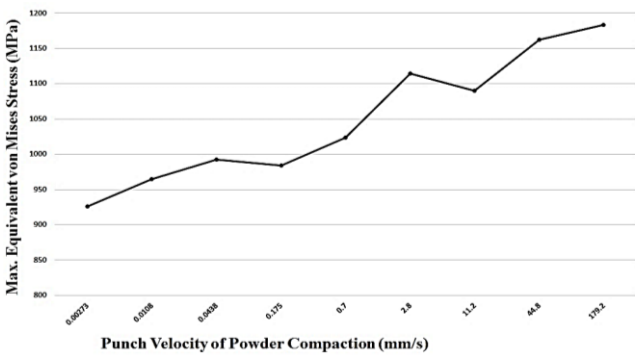

Fig. 3 Max. Eq. von Mises stress change via punch velocity

The equivalent of reaction forces acting on to the punch during compactions were given in Fig. 4. Compared with Fig. 3, a similar trend and increasing ratio in the graph was observed. This similar behavior showed that the Max. Eq. stress occurred in the elements that were contacting or positioning very close to punch, and there were no stress concentration caused by using different diameters of particles. It can be concluded that if it was intended to achieve a net or nearly net shape green body, the relation between compaction velocity and compaction force has be considered in industrial application.

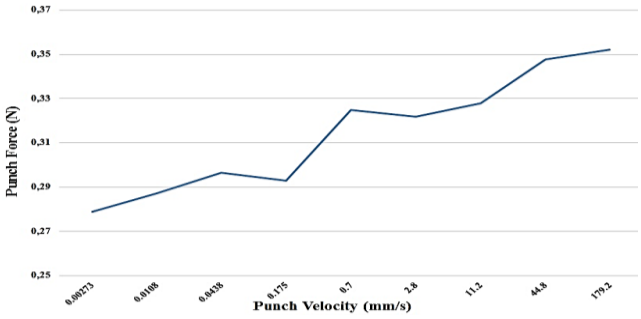

Fig. 4 Punch Force vs Punch velocity of 4140 steel powder compaction

After the Max. Eq. stress had been obtained from the punch zone, the stress distribution of particles according to the distance from punch to bottom of die was investigated and the stress distribution via compaction velocity plotted in Fig. 5. Stress distributions have lower values at the elements that were close to bottom of die. Stress values were increasing due to getting closer to the punch. Besides, stress values of elements also rose up by the compaction velocity. Elements those were in contact with bottom of die exposed 400-600 MPa Eq. von Mises stress at 0.00273-0.175 mm/s compaction velocity range. The Eq. von Mises stress value reaches 1000-1200 MPa at 0.3-0.5 mm far from the bottom in 179.2 mm/s compaction velocity. The fact that there was so much difference between these stress values, die height or part length be-came important parameter of powder compaction.

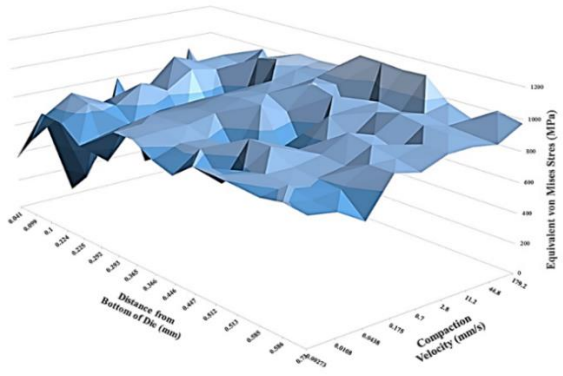

Fig. 5 Eq. von Mises change of different compaction velocities via distance from punch

In Fig. 6 Max. Eq. von Mises stress of different compaction velocities were shown via die height. The data collected from 20 elements that were in particle-die contact. There were so many values obtained from the MPFEM analyses, the data plotted as trend lines to have a more clear understanding. It was obvious that the stress distribution has a parabolic trend from punch to bottom of die. Almost in all different compaction velocities, the Eq. von Mises stress shows a drastic de-crease, and values became 60-70%

smaller from top to down of die. This decrease shows that die height has to be considered in compaction processes because some particles may not be bonding each other without sintering. By the time, in-crease of compaction velocity also increases the gap between the stress values of particles from top to down. In 179.2 mm/s analyses the Eq. von Mises stress parabolically decreases and bottom particles expose one third of the top particles.

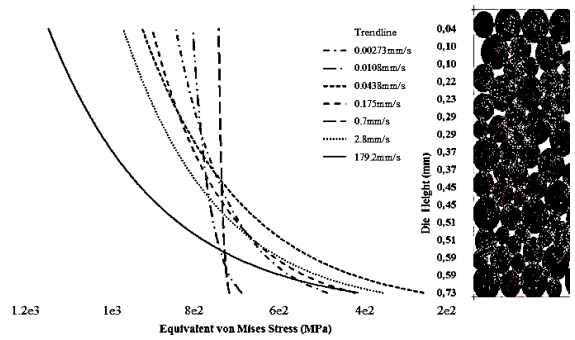

Fig. 6 Trends of Equivalent von Mises Stress via die height varying compaction velocities

Another aim of this study was to investigate the behavior of high RD compaction of AISI4140 powders. By the help of appropriate random distributed particles of different diameter, MPFEM analyses of this study have accomplished 95% RD. Most of the graphs plotted in Fig. 7 have peak points. The peak values of Max. Eq. von Mises stresses were be-tween 1000-1200 MPa while the final values of stresses came out in a range of 900-1100 MPa. It can be easily seen that the maximum values of stresses have been obtained from the earlier stages of compaction.

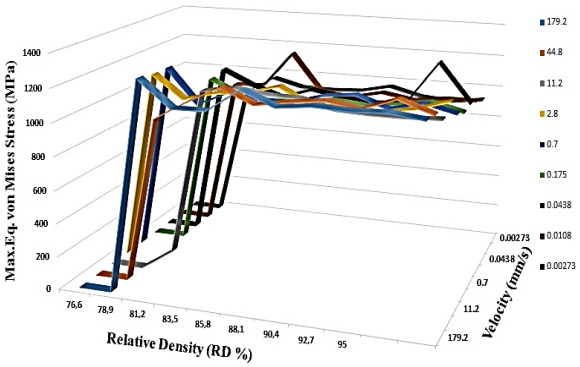

Fig. 7 RD effect on Max. Eq. von Mises Stress

Increasing velocity has a contribution on the max.-stress values obtained in low RD%. 11.2, 44.8 and 179.2 mm/s analyses show an obvious stress increase in the early stages. These stages can be defined as rearranging stages of particles. The final Max. Eq. von Mises stress of those MPFEM analyses have resulted in less values. Particles were re-arranging in the beginning of the compaction in other words they try to move other positions in order to fill the voids of die. The rearranging can be seen in most compaction analyses [2, 4, 30]. Especially, brittle material particles may deform or fracture before the final stage. It can be concluded that the particle size distribution have effects on peak stress of compaction.

The stress distribution of the particles of different diameters those were not in contact with die and punch were shown in Fig. 8. The Eq. von Mises stress scale shown in the left part of Fig. 8 was varying between 10 and 1500 MPa, indicating the large range of stress applied on the elements in such small volume. These stresses show agreement with iron or iron based materials in literature [8, 30, 31].

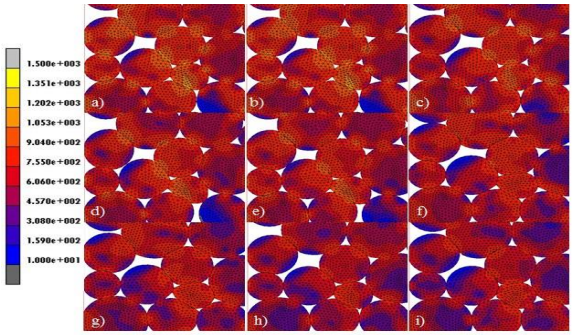

Fig. 8 Stress distribution of particles in three different diameters, a - 179.2, b - 44.8, c - 11.2, d - 2.8, e - 0.7, f - 0.175, g - 0.0432, h - 0.0108, i - 0.00273 (velocities are mm/s)

The stress values obtained from the elements of 0.00278 mm/s have a range between 10 and 1053 MPa, while over 1350 MPa stress values can be seen in 2.8/11.2/44.8/179.2 mm/s analyses. Particles of 25 µm in radius (small particles) were deformed more than other particles. The other particles, 35 µm (middle particles) and 45 µm (bigger particles) in radius also deformed but defining detailed conclusions cannot be easy from visual inspection.

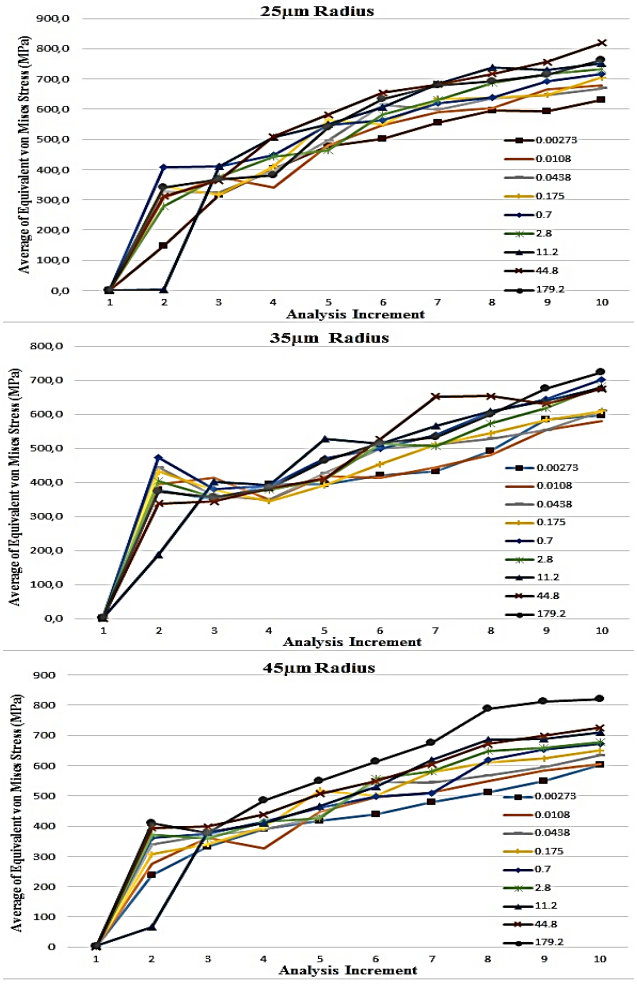

Fig. 9 Average of Eq. von Mises stress of different particles

In Fig. 9 Average of von Mises stress of all particles was shown. Data of all three groups of particles were selected and plotted via compaction velocities.

All three kinds of particles show similar trends. The stress data began to come out by the second increment and average of von Mises stress values for small particles were around 300 MPa, 400 MPa for middle particles and 350 MPa for big particles. At the final increment, average stresses reach a range of 580-820 MPa. Small and big particles exposed to 820 MPa in 179.2 mm/s and the lowest stresses obtained from the analysis of 0.00273 mm/s compaction velocity. In order to get a deeper investigation and compare particles with each other, stress graphs of three particles plotted for each compaction velocity and given in Fig. 10. It can be seen from the Fig. 10, except 179.2 mm/s compaction velocity analysis, average of Eq. von Mises stresses of small particles shows the highest values compared to other particles.

Similarly most of the images state big particles as the second highest stress exposed particles. After the 5th increment which corresponds 85.8% RD, small particles come out with the greatest values, therefore we can say if the compaction process intended to reach more than 85% RD the geometric composition of particles has an active role.

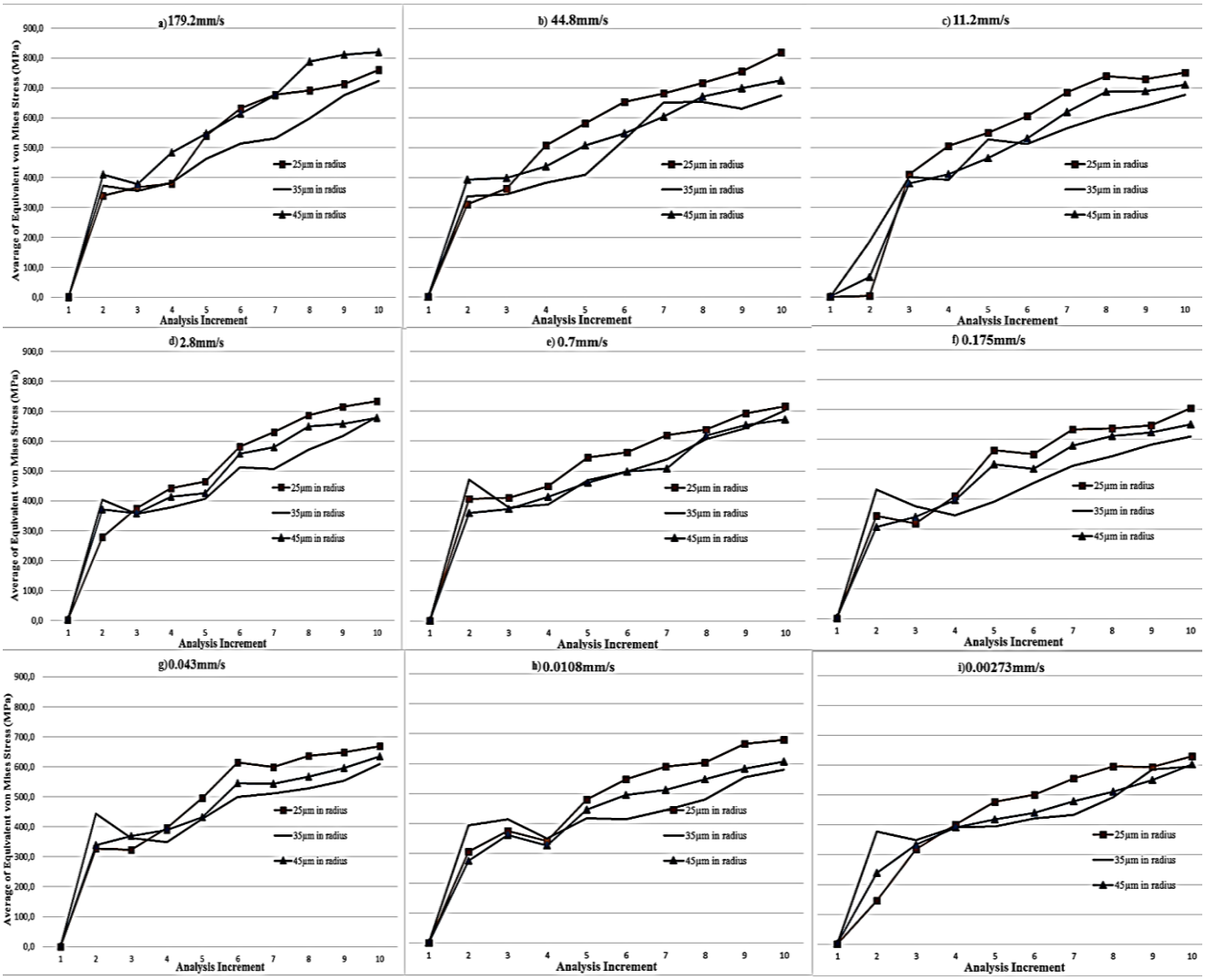

Fig. 10 Stress comparison of small, middle and big particles

4. Conclusion

In this study, compaction behavior of AISI 4140 steel powder investigated by MPFEM. The Equivalent von Mises stress distribution and visual inspection of powder compaction analysis performed with nine different compact tion velocity in order to achieve high RD green density of 95%. Following conclusions obtained from this study;

1. The force required to displace the punch increases by the increase of compaction velocity. In order to achieve high RD, stress value increases by 2% against every fourfold increase in velocity.

2. Respectively, more stresses obtained from the particles that were close to punch. The stress trend lines decrease parabolically by the particles located from punch to bottom of die. Attention should be paid to the parabolic change trend that increases with high RD values.

3. Maximum values of Eq. von Mises stresses occur during the rearrangement of the particles. This was particularly important in order to understand whether the particles were fractured in the initial stages of compaction according to the brittle behavior of the material.

4. From Fig. 10 Examination of average Eq. von Mises stresses during MPFEM analyses showed that small particles (25 µm in radius) exposed the highest stress values. Big particles (45 µm in radius) came after the small particles

and middle particles (35 μm in radius) were the last.

5. In order to achieve required final RD, the force applied by the punch has to be considered via different compaction velocities in industrial applications.

6. As well as die height has a negative effect on the stress distributions of particles, compaction velocity also disrupts the homogenous stress distribution.

References

1. **Han, P.; An, X.; Zhang, Y.; Huang, F.; Yang, T.; Fu, H.; Yang, X.; Zou, Z.** 2017. Particulate scale MPFEM modeling on compaction of Fe and Al composite powders, Powder Technology. 314: 69–77. http://dx.doi.org/10.1016/j.powtec.2016.11.021.
2. **Hasan, M.; Zhao, J.; Huang, Z; Chang, L.; Jiang, Z.** 2018. Analysis of sintering and bonding of ultrafine WC powder and stainless steel by hot compaction diffusion bonding, Fusion Engineering and Design. 133: 39-50. https://doi.org/10.1016/j.fusengdes.2018.05.076.
3. **Navarro, G.; Taleghani, M. A.; Torralba, J. M.** 2013**.** Pressed and sintered AISI 4140 PM low alloy steel from gas atomised powders, Powder Metallurgy, 56(1): 11-13 https://doi.org/10.1179/0032589912Z.00000000087.
4. **Sanborn, B.; Song, B.; Thompson, A.; Reece, B.; Attaway, S.** 2017. High strain rate tensile response of A572 and 4140 steel, Procedia Engineering. 197: 33-41. https://doi.org/10.1016/j.proeng.2017.08.079.
5. **Patil, C. K.; Shisode, S. P.; Shrigandhi, G. D.; Dhokane, N. T.** 2017. Tribological analysis of SAE 4140 steel, International Journal of Current Engineering and Technology, Special Issue-7 (March 2017). E-ISSN 2277 – 4106, P-ISSN 2347 – 5161.
6. **Jeong, J. H.; Ryu, S. K.; Park, S. J.; Shin, H. C.; Yu, J. H.** 2015. Analysis of iron powder design for compaction process, Computational Mat. Science. 100: 21–30. http://dx.doi.org/10.1016/j.commatsci.2014.11.028.
7. **Pavier, E.; Doremus, P.** 1999. Triaxial characterization of iron powder behavior, Powder Metallurgy. 42(4):345-352. https://doi.org/10.1179/003258999665693.
8. **Kang, C. S.; Lee, S. C.; Kim, K. T.; Rozenberg, O.** 2007. Densification behavior of iron powder during cold stepped compaction, Materials Science and Engineering A. 452–453 (2007) 359–366. https://doi.org/10.1016/j.msea.2006.10.113.
9. **Rahmaan, T.; Bardelcik, A.; Imbert, J.; Butcher, C.; Worswick, M. J.** 2016. Effect of strain rate on flow stress and anisotropy of DP600, TRIP780, and AA5182-O sheet metal alloys, International Journal of Impact Engineering 88: 72–90. http://dx.doi.org/10.1016/j.ijimpeng.2015.09.006.
10. **Wang, S.; Zheng, Z.** 2017. Discrete element method for high-temperature spread in compacted powder systems, Particuology 31: 49–53. http://dx.doi.org/10.1016/j.partic.2016.02.005.
11. **Luo, B.; Li, M.; Wang, G.; Tan, F.; Zhao, J.; Sun, C.** 2017. Strain rate and hydrostatic pressure effects on strength of iron, Mechanics of Materials. 114: 142–146. https://doi.org/10.1016/j.mechmat.2017.08.001.
12. **Gustafsson, G.; Nishida, M.; Häggblad, H.-Å.; Kato, H.; Jonsén, P.; Ogura, T.** 2014. Experimental studies and modelling of high-velocity loaded iron-powder compacts, Powder Technology 268: 293–305. http://dx.doi.org/10.1016/j.powtec.2014.08.060.
13. **Das, A.; Ghosha, M.; Tarafdera, S.; Sivaprasada, S.; Chakrabarti, D.** 2017. Micro mechanisms of deformation in dual phase steels at high strain rates, Materials Science & Engineering A 680: 249–258. http://dx.doi.org/10.1016/j.msea.2016.10.101.
14. **He, Y.; Evans, T.J.; Yu, A.B.; Yang, R.Y.** 2017. DEM investigation of the role of friction in mechanical response of powder compact, Powder Technology 319: 183–190. https://doi.org/10.1016/j.powtec.2017.06.055.
15. **Irazábal, J.; Salazar, F.; Oñate, E.** 2017. Numerical modelling of granular materials with spherical discrete particles and the bounded rolling friction model. Application to railway ballast, Computers and Geotechnics 85: 220–229. http://dx.doi.org/10.1016/j.compgeo.2016.12.034.
16. **Güner, F.; Sofuoglu, H.; Cora, Ö. N.** 2016. An investigation of contact interactions in powder compaction process through variable friction models, Tribology International 96: 1–10. http://dx.doi.org/10.1016/j.triboint.2015.12.016.
17. **Han, P.; An, X.; Wang, D.; Fu, H.; Yang, X.; Zhang, H.; Zou, Z.** 2018. MPFEM simulation of compaction densification behavior of Fe-Al composite powders with different size ratios, Journal of Alloys and Compounds 741: 473-481. https://doi.org/10.1016/j.jallcom.2018.01.198.
18. **Leclerc, W.** 2017. Discrete element method to simulate the elastic behavior of 3D heterogeneous continuous media, International Journal of Solids and Structures 121: 86–102. http://dx.doi.org/10.1016/j.ijsolstr.2017.05.018.
19. **Leclerc, W.; Haddad, H.; Guessasma, M.** 2017. On the suitability of a Discrete Element Method to simulate cracks initiation and propagation in heterogeneous media, International Journal of Solids and Structures 108: 98–114. http://dx.doi.org/10.1016/j.ijsolstr.2016.11.015.
20. **Güner, F.; Cora, O.N.; Sofuoglu, H.** 2018. Effects of friction models on the compaction behavior of copper powder, Tribology International 122: 125–132. https://doi.org/10.1016/j.triboint.2018.02.022.
21. **Dong, K.; Wang, C.; Yu, A.** 2015. A novel method based on orientation discretization for discrete element modeling of non-spherical particles, Chemical Engineering Science 126: 500–516. http://dx.doi.org/10.1016/j.ces.2014.12.059
22. **Lu, G.; Third, J.R.; Müller, C.R.** 2015. Discrete element models for non-spherical particle systems: From theoretical developments to applications, Chemical Engineering Science 127: 425–465. http://dx.doi.org/10.1016/j.ces.2014.11.050.
23. **Höhner, D.; Sirtz, S.; Scherer, V.** 2015.A study on the influence of particle shape on the mechanical interactions of granular media in a hopper using the Discrete Element Method, Powder Technology 278: 286–305. https://doi.org/10.1016/j.powtec.2015.02.046.
24. **Moghaddam, M.; Darvizeh, R.; Davey, K.; Darvizeh, A.** 2018. Scaling of the powder compaction process, International Journal of Solids and Structures, 144–145, 192-212. https://doi.org/10.1016/j.ijsolstr.2018.05.002.

25. **Zhang, Y.; Chen, Q.; Guillemot, G.; Gandin, C.-A.; Bellet, M.** 2018. Numerical modelling of fluid and solid thermomechanics in additive manufacturing by powder-bed fusion: Continuum and level set formulation applied to track- and part-scale simulations. Comptes Rendus Mecanique 346: 1055–1071. https://doi.org/10.1016/j.crme.2018.08.008.
26. **Güner, F.; Cora, O.N.; Sofuoglu, H.** 2015. Numerical modeling of cold powder compaction using multi particle and continuum media approaches, Powder Technology 271: 238–247. http://dx.doi.org/10.1016/j.powtec.2014.11.008.
27. **Huang, F.; An, X.; Zhang, Y.; Yu, A. B.** 2017. Multi-particle FEM simulation of 2D compaction on binary Al/SiC composite powders, Powder Technology 314: 39–48. http://dx.doi.org/10.1016/j.powtec.2017.03.017.
28. Marc 2016 Volume A: Theory and User Information, User Documentation: Copyright 2016 MSC Software Corporation, U.S. Patent 9,361,413.
29. **Groover, M. P.** 2010. Fundamental of Modern Manufacturing: Materials, Process and System, fourth ed, John Wiley and Sons, USA, 2010.
30. **Cristofolini, I; Molinari, A.; Pederzini, G.; Rambelli, A.** 2016 Study of the uniaxial cold compaction of AISI 316L stainless steel powders through single action tests., Powder Technology 295: 284–295. http://dx.doi.org/10.1016/j.powtec.2016.03.045.
31. **Harthong, B.; Jérier, J.-F.; Dorémus, P.; Imbault, D.; Donzé, F.-V.** 2009. Modeling of high-density compaction of granular materials by the Discrete Element Method, International Journal of Solids and Structures 46: 3357–3364. https://doi.org/10.1016/j.ijsolstr.2009.05.008.

F. Güner

NUMERICAL INVESTIGATION OF AISI 4140 POWDER HIGH RELATIVE DENSITY COMPACTION IN TERMS OF COMPACTION VELOCITY

S u m m a r y

In this study high relative density compaction of AISI 4140 steel powder compaction numerically investigated via different compaction velocities using Multi Particle Finite Element Method (MPFEM). 2D Analyses performed by three different particle geometry; 25, 35 and 45 μm in radius. Particle size effect also investigated via high relative density and compaction velocity. von Mises Power law evaluated for AISI 4140 steel powder and utilized to analysis. Results were plotted both in visually and graphically in aim to show effect of relative density, particle size, contact interactions and compaction velocity. The stress distribution through the height of die revealed out. A four-fold increase in compaction velocity increase the Equivalent von Mises stress 2% where the stress value can reach up to 3 times the yield stress. Stress values along the punch to the bottom of the die show a parabolic tendency with compaction velocity increase.

Keywords: AISI 4140, MPFEM, powder compaction, compaction velocity, high relative density.

Received March 02, 2019
Accepted February 03, 2020